coatings

MDPI

Article

Effect of Surface Modification on the Primary Stability of Dental Implants by Plasma Oxidation and Storage Treatment

Fei Sun [1], Shao-Jie Li [2], Xin-Chang Li [3], Lei Wang [1], De-Chun Ba [1], Gui-Qiu Song [1], Chuan-Sheng Sun [4] and Zeng Lin [1,5,*]

1 School of Mechanical Engineering and Automation, Northeastern University, Shenyang 110004, China; 1810132@stu.neu.edu.cn (F.S.); wanglei1880407@sina.com (L.W.); dchba@mail.neu.edu.cn (D.-C.B.); gqsong@mail.neu.edu.cn (G.-Q.S.)
2 Shanghai Institute of spacecraft Equipment, Shanghai 200240, China; sjli_sise@163.com
3 WEGO JERICOM Biomaterials Co., Ltd, Weihai 264210, China; newly-lxc@163.com
4 WEGO Holding Co., Ltd., Weihai 264210, China; msw2011@126.com
5 Key Laboratory of Implant device and Interface Science of Liaoning province, Northeastern University, Shenyang 110819, China
* Correspondence: zlin@mail.neu.edu.cn; Tel.: +86-24-8367-6945

Received: 5 June 2020; Accepted: 28 June 2020; Published: 29 June 2020

Abstract: Plasma oxidation could produce an oxidized surface, resulting in a graded TiO_{2-x} film layer and significantly improving dental implant hydrophilicity and biocompatibility. Unfortunately, these features are gradually lost by the influence of the environment. In this study, alkali storage was used to improve these characteristics at room temperature. Titanium samples were divided into sandblasting acid-etching (SLA), oxidation (SLA samples that were oxidized), and storage (SLA samples that were oxidized and stored in 0.1 mol/L NaOH solution) groups. We measured the surface properties of each group, including the roughness, chemical composition, and hydrophilicity of these materials. We investigated the effects of titanium storage on cell responses, including cell attachment, proliferation, differentiation. We also investigated the osseointegration of the stored titanium implants. The results showed that the storage process maintains the superhydrophilic properties of oxidation treatment. Oxidized samples promoted cell responses. The descending order of biocompatibility was storage > oxidation > SLA. Furthermore, oxidation and alkali storage had significant effects on bone growth at the early stage of the implant. These results suggested that alkali storage can suitably maintain the surface characteristics of plasma oxidation, and the combination of oxidation and storage treatment can improve the primary implant stability.

Keywords: dental implant; plasma oxidization; alkali treatment; superhydrophilic surface; osseointegration

1. Introduction

Titanium (Ti) has been used for a long time as a medical implant material due to its favorable characteristics, including excellent mechanical properties, corrosion resistance, and biocompatibility [1,2]. However, the recovery period after dental implantation can be as long as 3–6 months [3]. This is a crucial phase since there is a high risk of early implant failure due to poor osseointegration. To strengthen the area between titanium implants and bone, numerous researchers have focused on improving the surface biological activity of implant materials to attain better osseointegration in a shorter time.

The improvement of surface biological activity results from changes in morphology and surface chemical properties. At present, micron-scale sandblasting acid-etching morphology is the most commonly used and widely studied, and its suitable micron-scale rough morphology is conducive to cell adhesion and growth [4]. In addition, changing the surface composition through surface modification is another method to improve the biological activity on the surface, including the use of hydroxyapatite composite coatings [5], and Ag/Zn ion injections with antibacterial activity [6]. The aim is to regulate cell and protein response characteristics by altering the composition of surface elements. Plasma modification and implantation are recent developments in surface modification that can be used to enhance the surface properties of materials without altering their original morphology. Therefore, there is no risk of the tissue being inflamed due to the force exerted as the coating falls off. Using oxygen plasma treatment can improve the osseointegration of Ti and enhance corrosion resistance in simulated body environments and promote the adhesion, proliferation, and differentiation of human bone marrow mesenchymal stem cells [7,8]. In our previous work, we developed vacuum plasma oxidation and a low energy oxygen ion implantation technique, which has the advantage of guaranteeing uniformity, especially for 3D implant devices, and has the advantage of possessing superhydrophilic properties [9].

However, the highly active, superhydrophilic surface was very sensitive and was affected by the surroundings, resulting in degradation. This degradation process may come from the adsorption of hydrocarbons, and surface-treated implants may take a long time for clinical applications, so some wet storing techniques were developed to solve this problem [10–12]. Therefore, changes in surface chemical properties and effects in stored procedures should also be considered. Studies have shown that the contamination of hydrocarbons on the surface of titanium materials is not conducive to the adhesion and proliferation of osteoblasts [13]. Indeed, the active surface, which has increased hydrophilicity and surface free energy, has resulted in an improved bone-implant contact (BIC) area at early stages of healing [14–19]. For smooth titanium materials, alkali-treated titanium without heat treatment had no bone-bonding ability due to the unstable reactive surface layer [20]. For SLA titanium materials, alkaline treatment at normal temperature shown good wettability and biocompatibility [11].

Many alkali storage methods are directed to SLA surfaces, but the effects on plasma oxidized TiO_{2-x} surfaces are for further study. In this study, we measured the superhydrophilic surface properties of oxidized implant surfaces by alkali storage at room temperature. Furthermore, cell responses—including cell adhesion, proliferation, and differentiation—were examined on oxidized samples stored in alkali solution. The effects of implant removal torque and osseointegration rate were studied by animal experiments. Thus, we propose a method for improving the primary stability of titanium implants between bones and the implant surface. The results of this study provide the basis for the treatment and protection of an ideal dental implant surface.

2. Materials and Methods

2.1. Specimen Preparation

The samples include SLA Ti disks (15 mm diameter and 1.5 mm thickness) and SLA-treated dental implants. The SLA surface was treated by sandblasting with TiO_2 followed by acid etching, and the mixed acid contained 60% H_2SO_4, 10% HCl, and deionized water. The specimens were commercial materials commonly used for dental implants. Then, the samples were treated with oxygen plasma, resulting in the generation of superhydrophilic TiO_{2-x} thin films. By using radio-frequency (RF) and direct current (DC) enhanced chemical vapor deposition (CVD) equipment (RF-500, Cross-Tech Equipment Co., Ltd., Shanghai, China), the oxygen plasma produced by vacuum glow discharge bombarded the surface of SLA samples. The optimum parameters of plasma oxidation treatment and specific technological processes were described in detail in our previous work [9]. Ti disk samples were divided into three groups: SLA, oxidation (SLA samples that were oxidized), and storage (SLA samples that were oxidized and stored in 0.1 mol/L NaOH solution), and the samples were exposed

to room temperature and atmospheric pressure for 10 days. Ti dental implant samples were divided into two groups: SLA and storage, and the samples were prepared for use in animal experiments. All samples are subjected to high temperature disinfection and washing before the experiment.

2.2. Surface Characterization

The surface topography was evaluated by scanning electron microscopy (SEM) (INSPECT F50, FEI, Eindhoven, The Netherlands). Surface roughness analysis of SLA samples and Oxidation samples was carried out using a surface roughness measurement device (MiCROMEASURE2, STIL, Aix, France). The sampling area was set as 100 × 100 μm^2, and the step size was 1.0 μm. The parameters for numerically characterizing the roughness were the arithmetic mean of the absolute values of roughness (S_a).

Surface chemistry and the depth profiles of the chemical composition were characterized by XPS (ESCALAB250, Thermo-VG, Waltham, MA, USA) with monochromatic Al Kα (1486.7 eV), and the parameters used to operate the sputtering gun were as follows: XR5 Gun-500 μm (15 kV, 150 W), test mode (500 μm). Typical XPS spectra were recorded in a vacuum with pressure greater than 6.0 × 10^{-8} mbar and 20 eV pass energy. The etching rate was 0.1 nm/s. The spectra (Ti2p and O1s) were curve-fitted using a computer-assisted Lorentzian–Gaussian peak model. Four chemical states of the titanium atom, including Ti^0 (Ti), Ti^{2+} (TiO), Ti^{3+} (Ti_2O_3), and Ti^{4+} (TiO_2), were distinguishable in the Ti2p spectra. The reference binding energies for Ti, TiO, Ti_2O_3, and TiO_2 were obtained from previous research [9].

The contact angles were measured by the θ/2 method on a SL200B tensiometer (Kino, Shanghai, China), and the test liquid was 1 μL of DI H_2O. SLA and oxidation samples were rinsed with 0.1 mol/L NaOH solution for 10 s. Then the three groups of samples are washed with deionized water and dried before measuring the water contact angle.

2.3. Cell Responses

In the experimental cell culture process, mouse cranial MC3T3-E1 cells were placed in α-MEM culture medium containing 10% fetal bovine serum and cultured in a constant temperature incubator at 37 °C, 95% humidity, and 5% CO_2. The liquid was changed for 2–3 days and passed for 3–4 days (to allow the cells to grow to 90% confluence). Cells were treated before any detection to select the growth state when the cell morphology was best. The cells in the log phase of growth were plated and tested, and the liquid change was conducted the day before. For the cell counting method, the cells were washed twice with phosphate buffered saline (PBS) and trypsinized until the cells were retracted but not suspended. The medium was then added to terminate digestion, and air was repeated blown through the pipette until the cells were suspended. The cells were transferred to a centrifuge tube for centrifugation (1000 rpm, 5 min), the supernatant was then removed, and the medium was added. The cell pellet was gently pipetted into a cell suspension of uniform density and count.

2.3.1. Cell Attachment Assay

The osteoblast adhesion spread test was divided into three time points: 6, 24, and 48 h. Two samples per group were collected at each monitoring time point. The inoculation density was 5 × 10^4/mL, and 1 mL of the culture solution was added. The plate was replaced at each time point, washed with PBS, and fixed with glutaraldehyde at a concentration of 2.5% at 40 °C overnight. The fixative solution was removed, rinsed twice with PBS for 10 min, dehydrated with an ethanol series, and dried at the CO_2 critical point. Finally, the adhesion and spreading morphology of osteoblasts were observed by SEM.

2.3.2. Cell Proliferation Assay

Three 12-well culture plates were used for monitoring at 4 time points, including 1, 3, 5, and 7 days, and each group had cells inoculated at four time points. Samples of each of the three sets were

placed in a 12-well culture plate and inoculated at a cell density of 3×10^4/mL. Next, 1 mL of the culture solution was added to each well, and the solution was changed every other day. At each time point, three samples from each group were removed and placed in a new 24-well plate and rinsed twice with PBS to remove nonadherent cells. Then, 800 μL of the culture medium and 200 μL of MTT reagent were added to each well, and the culture was continued for 4 h in an incubator. After 4 h, the liquid in each well was aspirated and rinsed twice with PBS. Next, 1 mL of dimethyl sulfoxide (DMSO) was added to each well and allowed to dissolve for 10 min; then, 200 μL of solution was then injected into each well of 96-well plates and detected by enzyme-linked immunosorbent assay during which the absorbance value (OD value) was measured at a wavelength of 490 nm.

2.3.3. Cell Differentiation Assay

Using the alkaline phosphatase (ALP) activity test, three samples were tested at each time point for each set of samples at 3, 5, 10, and 15 days. The cell seeding density was 3×10^4/mL, and 1 mL of the culture solution was added. The cells were changed overnight. The cells were changed to a new plate at each time point. After PBS rinsing, each well was separately diluted with trypsin for 3 min, PBS was blown, and the cell pellet was collected by centrifugation. Next, 50 μL of 0.3% Triton X-100 was added to freeze–thaw the cells repeatedly, and the cells were transferred to an EP tube. The supernatant was collected by centrifugation at 4 °C (12,000 rpm, 5 min). The OD values of each well were then determined as described in the alkaline phosphatase kit. The OD value of each well was determined according to the protein concentration (BCA) kit, a standard curve was drawn, and the protein concentration in each group was calculated according to the standard curve. Finally, alkaline phosphatase activity was calculated according to the formula in the alkaline phosphatase kit.

2.4. Animal Experiments

For the animal experiments, eight New Zealand white rabbits were used as the animal model. To evaluate the strength of the interface between the implant surfaces and bone, implants were divided into two groups: SLA samples and storage samples. Implants (n = 32) were randomly implanted into the left and right mandibles of the rabbits, with two implants on each side. All animal procedures and experimental protocols were approved by the Institutional Animal Experiment Ethics Committee of Jiamusi University. All guidelines regarding the care of animals were strictly followed. For the surgical procedure, the animals received anesthesia with a xylazine hydrochloride injection (Lumianning, Jilin, China; dosage: 18 mg/kg) administered intramuscularly. A round bur was used to locate the cortical bone, and then a fissure bur was used drill to set the depth. Finally, the implant was screwed into the bone until all threads entered. Subsequently, the animals were fed a light diet for one week. Both implants were observed and evaluated for failure and inflammation after implantation.

The animals were sacrificed 2 weeks and 4 weeks after implantation. Implant removal torques of both implants were obtained by biomechanical testing. The specimens used for the removal torque test were removed and fixed on the stage. Then, the removal torque value was recorded with a torque tester (Pake 1 N·m, Pake Tool Factory, Zhejiang, China). In addition, the bone-implant contact (BIC) ratios of both implants were measured. Sample preparations for histological analysis were followed by fixing, methyl methacrylate embedding, ultramicrotome sectioning, grinding, and staining with 0.05% toluidine blue. The stained slides were observed under an optical microscope (Olympus BX41, Tokyo, Japan).

The BIC ratio was calculated by Equation (1)

$$\text{BIC } (\%) = N/T \times 100\% \quad (1)$$

where, N is the sum of the bone-implant contact and T is the total length of the thread of the implant.

2.5. Statistical Analysis

All of the experiments were performed multiple times, and at least three samples were used for each test group in each experiment. Statistical analyses were performed using the one-way analysis of variance method. The significance level was $\alpha = 0.05$; any P-value below 0.05 was considered statistically significant. SPSS 17.0 statistical software was used to statistically analyze the protein adsorption rate of the four titanium samples in this experiment.

3. Result

3.1. Surface Characterization

As shown in Figure 1, the surface topography was evaluated by SEM (INSPECT F50, FEI, Eindhoven, The Netherlands). No significant differences were found among SLA, oxidation, and storage samples, and all maintained the original micro/nano hole nesting structure on the sample surface. Surface roughness was measured using a surface roughness measurement device. A small difference in roughness was observed among three groups. The surface roughness of the three groups of samples is 0.429 ± 0.029 μm (SLA), 0.471 ± 0.049 μm (oxidation), and 0.460 ± 0.054 μm (storage), respectively. There are significant differences among the three groups ($P < 0.05$).

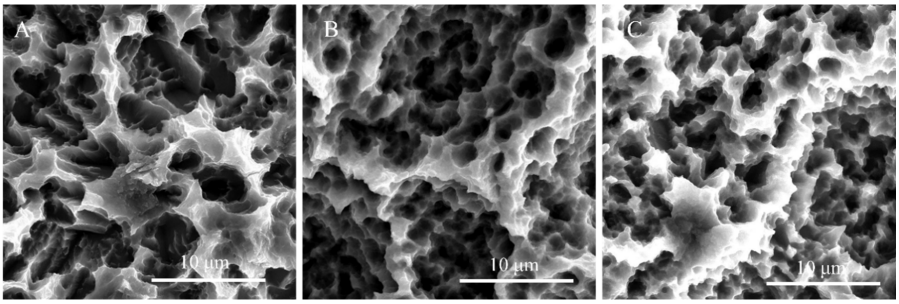

Figure 1. Morphology of Ti samples before and after treatment: (**A**) SLA, (**B**) Oxidation, (**C**) Storage.

Figure 2 shows the variation of Ti^{4+}, Ti^{3+}, Ti^{2+}, and Ti of the plasma oxidation surface regarding the depth from the top surface. On the surface of the oxide film, the main components are Ti^{3+} and Ti^{4+}. When the depth reached 50 nm, pure Ti began to increase in depth, which implied that the typical TiO_{2-x} surface had a thickness of approximately 50 nm. It was clear that the gradual TiO_{2-x} surface had formed due to plasma oxidation on the dental implant device. There was no distinct interface (50–100 nm) between the top TiO_{2-x} surface and the implant substrate.

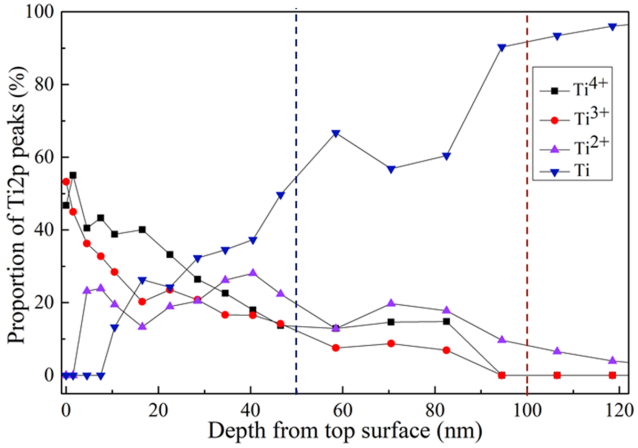

Figure 2. Proportion of different Ti valence states of the plasma oxidation surface in depth from the top surface.

Figure 3a shows a Ti2p pattern of the oxidation surface of fresh and stored samples. The Ti2p spectra were decomposed into four chemical states, including Ti^{0} (Ti), Ti^{2+} (TiO), Ti^{3+} (Ti_2O_3), and Ti^{4+} (TiO_2). It is implied that Ti^{4+} and Ti^{3+} stayed at the main valence state on the top TiO_{2-x} surface. In addition, according to the area of each peak, the proportion of each Ti valence is actually different. The proportion of Ti^{3+}2p3/2 on the surface of the sample stored in alkali solution was reduced by 6% compared to that of the fresh oxidized sample surface, whereas all the other proportions increased. The proportions of TiO_2 and Ti_2O_3 were 52.01% and 47.99%, respectively, in the alkali solution, while the corresponding ratios of the fresh oxidation surface were 46.74% and 53.26%, respectively. Both of the oxidized surfaces included mainly Ti^{4+} and Ti^{+3} components. Figure 3b shows a O1s pattern of the oxidation surface of fresh and stored samples. Different from the oxidation surface, for the storage surface, only three O1s spectral peaks were obtained after the Gauss peak fitting treatment. Regarding the O1s peaks, the peaks corresponding to TiO_2, Ti_2O_3, and the hydroxyl group (Ti–OH) had binding energies of 529.6, 530.3, and 531.7 eV, respectively. The oxygen on storage surface mainly existed in the form of TiO_2 and Ti_2O_3 in proportions of 44.42% and 40.77%. In addition to the absence or few C–O groups, the level of Ti–OH dropped after alkaline storage, from 22.90% to 14.84%.

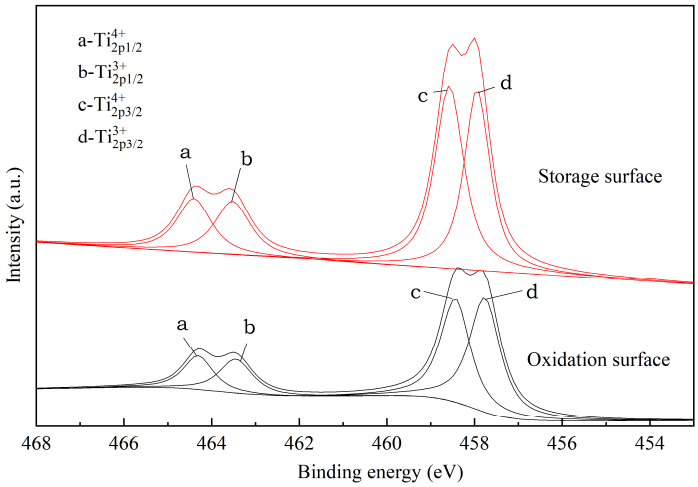

(**a**)

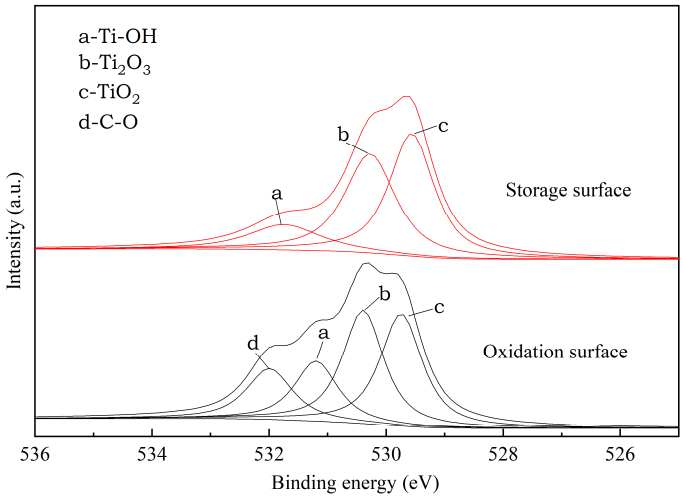

(**b**)

Figure 3. (**a**) Ti2p patterns and (**b**) O1s patterns on the oxidation surface of a Ti-sample before and after storage in alkali solution.

Figure 4a shows the hydrophilicity of the oxidized surface over time. Hydrophilicity gradually decreased, and the water contact angle increased. After 12 days, the contact angle exceeded 90 degrees. Figure 4b shows the contact angles of the three groups (SLA, oxidation, storage) after 10 days. From the results of this experiment, it can be seen that the surface of the SLA sample and the surface of the oxidation sample had similar contact angles and had no hydrophilic properties (contact angles of <45° are hydrophilic). The storage samples maintained the superhydrophilic property well (contact angles of <10° are superhydrophilic).

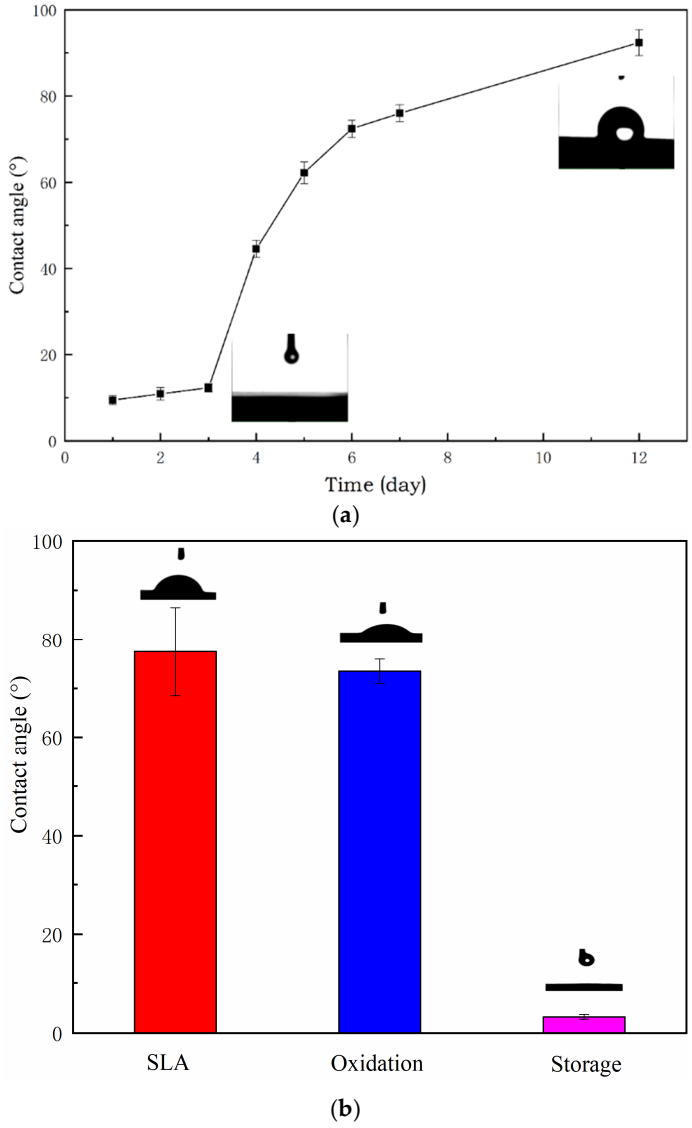

Figure 4. (**a**) Hydrophilic changes in the oxidized surface over time. (**b**)The contact angles of the three groups.

3.2. Cell Responses: Attachment, Proliferation, Differentiation, Morphology, and Morphometry

The filopodium structures of osteoblasts after 6, 24, and 48 h were observed on the sample surfaces of three groups by SEM at 5000× and 50,000× magnification, and are shown in Figure 5. At the first time point, the mouse cranial MC3T3-E1 cells on the surface of the three groups of samples began to stretch. The cell morphology of each group was not very different, and the cells exhibited a polygonal spindle and flat shape in 6 h. Cells spread and filled the entire field of vision in 24 h. The number of filaments and filopodia of cells on the surface also increased significantly and adhered firmly to

the surface of the rough titanium specimens. After 48 h, the three groups did not show significant differences. However, the number and stretches of filopodia were greater in the storage group.

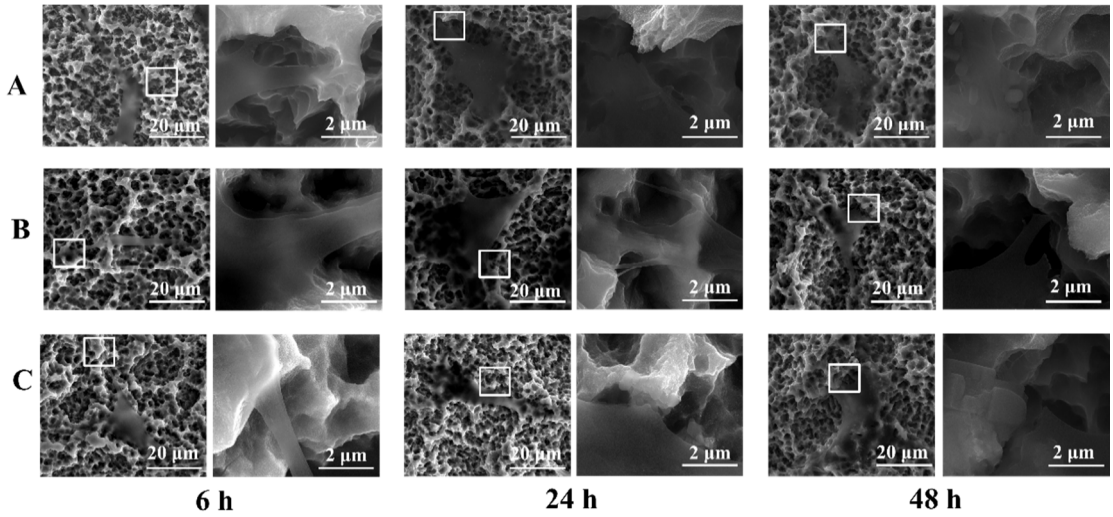

Figure 5. Adhesion and spread of cells on the sample surface after cell culture for 6, 24 and 48 h: (**A**) SLA, (**B**) oxidation, (**C**) storage.

The MTT results of each group varied with time, as shown in Figure 6a. After 1, 3, 5, and 7 days of cell culture, the number of osteoblasts in the three groups gradually increased with time. The absorbance (OD) values measured for the three groups were storage > oxidation > SLA. Differences in the absorbance among the groups were observed at day 1, while differences observed on day 3 were not significant. However, the OD values at days 5 and 7 were remarkably larger than those at the other time points. Intracellular alkaline phosphatase (ALP) activity is one of the most widely employed metrics for mid-stage osteogenic differentiation. The results of the ALP assay are shown in Figure 6b. The results of the ALP assay are similar to the results of the MTT assay of cell adhesion and proliferation. The ALP activity values measured at the three test points revealed the following trend: storage > oxidation > SLA.

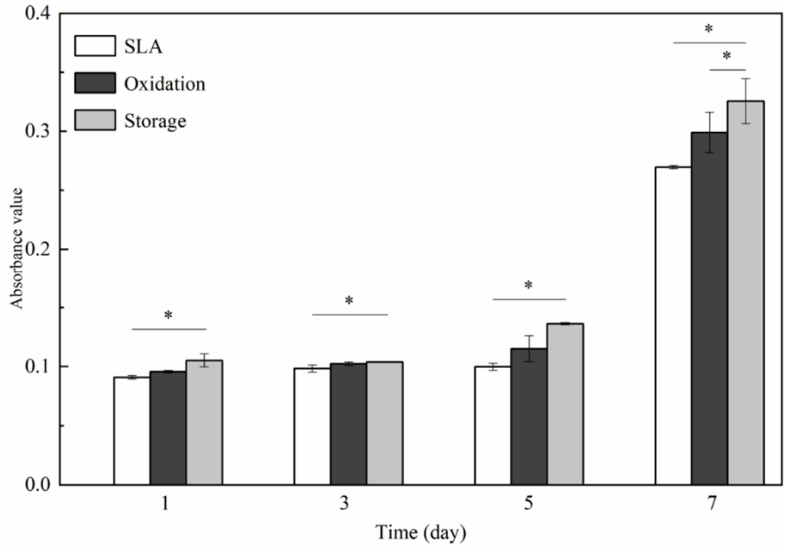

(**a**)

Figure 6. *Cont.*

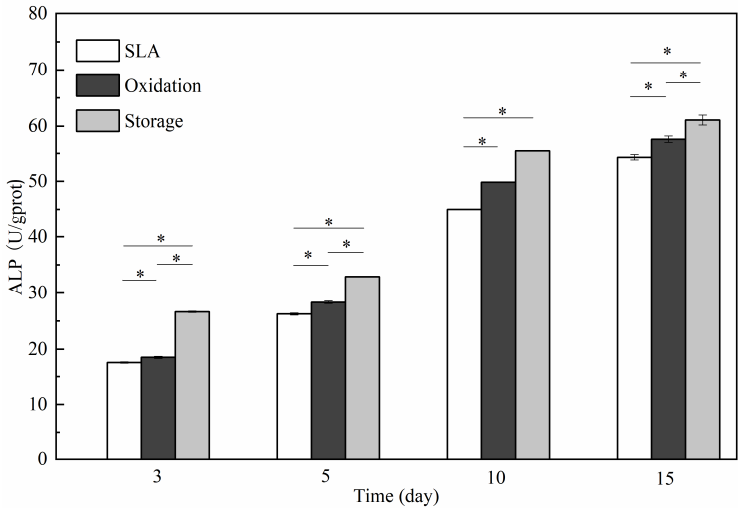

(**b**)

Figure 6. (**a**) OD values of the three groups of samples ($\overline{x} \pm s$, $n = 3$, * indicates $P < 0.05$ among groups); (**b**) ALP activity in the three groups of samples ($\overline{x} \pm s$, $n = 3$, * indicates $P < 0.05$ among groups).

3.3. Animal Experiment

Considering the above results, in animal experiments, implants were divided into two groups: SLA samples and storage samples. The removal torque value (RTV) and bone-implant contact (BIC) results of the two groups are shown in Figure 7a,b. Comparing the size of the removal torque between SLA and storage, the results showed that the surface treatment methods of the two implants were statistically significant at different implantation times ($P < 0.05$); the difference between the groups was statistically significant ($P < 0.05$). The storage implants had a higher RTVs and BIC ratios than the SLA implants.

The staining results of toluidine bone tissue showed that the Storage group (Figure 8B,D) exhibited better osseointegration than the SLA group (Figure 8A,C) at both 2 and 4 weeks. It can be observed from Figure 8A that there was a small amount of new bone formation on the surface of the implant. The new bone formation is mainly concentrated in the oblique wall of the implant thread and a small amount of new bone formation at the thread base. Figure 8B shows that trabeculae not only surround the oblique wall of the thread but are also generated at the bottom of the thread, with obvious contact ontogenesis. Figure 8C shows that the new bone extends from the bone matrix to the threaded cavity. There are more trabeculae in the middle of the threaded cavity, more newly formed bone at the bottom and sidewall of the thread, and a small amount of Haversian system canals in the threaded cavity. It can be observed from Figure 8D that the new bone is distributed in the oblique wall close to the mature bone. A large number of new bone formations is also present at the bottom of the thread, and a large area of new bone formation is also observed in the threaded cavity. More Haversian system canals can be seen in the implant socket bone wall and threaded cavity.

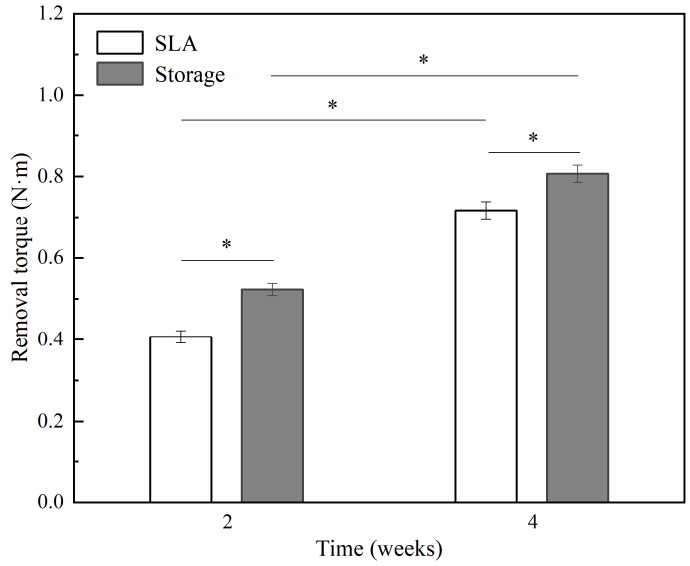

(**a**)

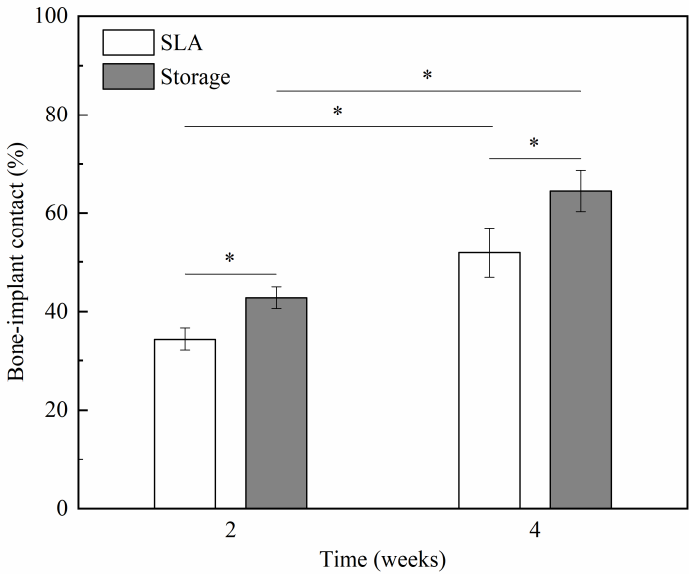

(**b**)

Figure 7. (**a**) Removal torque value results ($\overline{x} \pm s$, $n = 3$, * indicates $P < 0.05$ among groups); (**b**) Bone-implant contact results ($\overline{x} \pm s$, $n = 4$, * indicates $P < 0.05$ among groups).

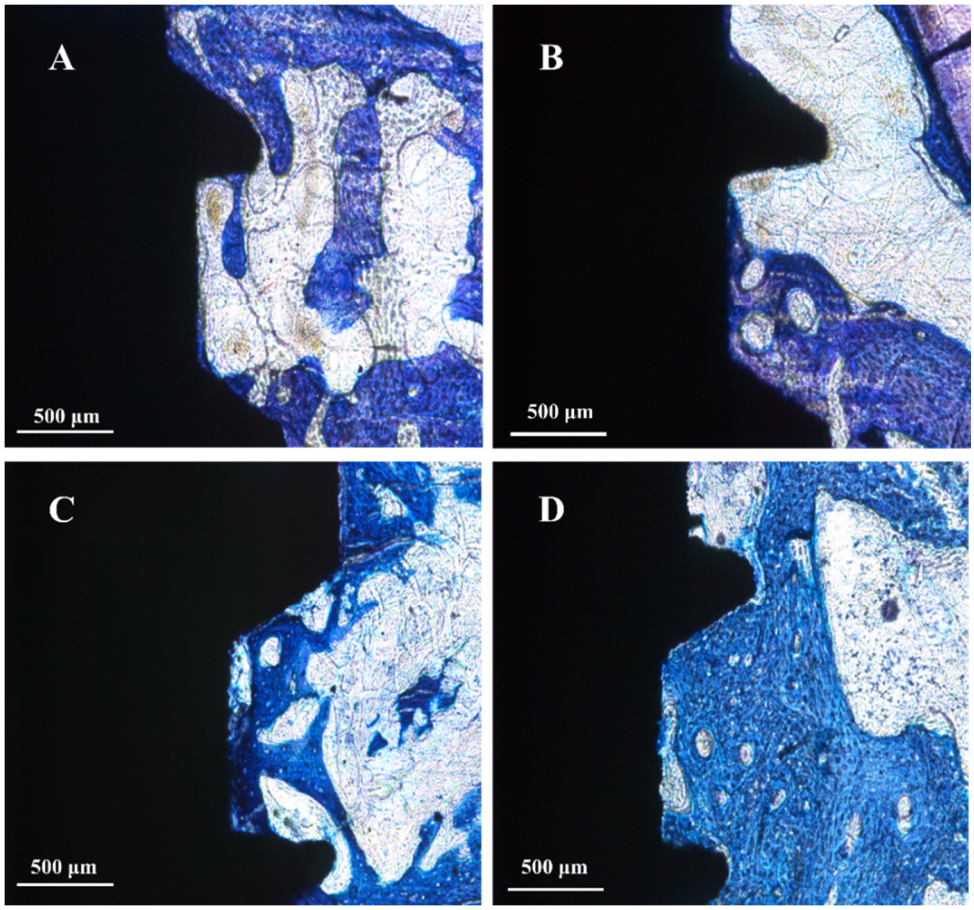

Figure 8. Toluidine blue staining results of bones: (**A**) SLA group after 2 weeks; (**B**) Storage group after 2 weeks; (**C**) SLA group after 4 weeks; (**D**) Storage group after 4 weeks, ×100.

4. Discussion

In our previous work, we provided a modified hydrophilic surface based on a vacuum plasma oxidation process while maintaining the SLA micro/nano compound microstructure of the dental implant surface [9,21,22]. However, some changes still appeared on the surface, as evidenced by the SEM images of the morphology of the samples shown in Figure 1. Samples after vacuum plasma oxidation treatment presented higher Sa values compared to SLA samples. When plasma oxidation treatment is carried out, there is a sputtering effect on the surface peak microstructure, and the surface micropores become rougher. This indicates that the increased rate of the surface interface area is larger than that of the SLA surface. This change is reasonable since the energetic particles will collide with the surface and then result in morphological changes during oxygen reactive particle implantation into the surface. In addition, we found that alkali storage has a surface roughness similar to oxidation. It was shown that alkali storage did not change the oxidized surface morphology at room temperature [11].

Figure 2 implied that Ti^{4+} and Ti^{3+} maintained the main valence state on the top TiO_{2-x} surface (50–100 nm), which showed a larger difference compared with the chemical composition of the SLA surface. A native oxidation surface was formed (very thin and loose approximately 4–6 nm) with a dominant Ti^{4+} valence state of Ti together with few Ti^{2+} and Ti^{3+} components [23]. The change in TiO_2 and Ti_2O_3 on the surface may be related to the higher reaction energy on the surface. Comparing the oxidized surface composition before and after storage (Figure 3a), the content ratios of Ti^{4+} and Ti^{3+} have small differences. A small fraction of the Ti^{3+} was oxidized and converted into Ti^{4+} after storage because Ti^{3+} was highly active. In addition, researchers [24] have found that SLA samples after storage treatment have a high surface chemical energy, which may be related to higher surface energy

and titanium dioxide conversion. Figure 3b shows a O1s pattern of the oxidation surface before and after storage. The decrease of Ti–OH groups was mainly due to the deprotonation and ion exchange of Ti–OH groups in the alkaline environment to form Ti–O–Na ion pairs [25]. The decrease of C–O groups after the alkaline solution treatment may be due to the removal of carbonate on the sample surface by the alkaline solution [11].

The superhydrophilic surface obtained by vacuum plasma oxidation treatment gradually disappears because hydrocarbons are adsorbed in the air [13]. It was reported that an active Ti component (such as Ti^{3+}) has a crucial role in hydrophilicity and related biological properties [22]. A large amount of Ti^{3+} can form a self-doped TiO_{2-x} structure, which can facilitate the formation of hydroxyl (–OH) upon excitation with visible light [26]. Figure 4 indicates that alkali rinsing cannot restore hydrophilicity; however, alkali storage is beneficial in protecting the TiO_{2-x} structure of the oxidized surface, thereby improving superhydrophilic properties. In addition, the alkali storage produced a higher surface pH, which is conducive to achieving superhydrophilicity [11]. These are different from SLActive surface. Research suggests that the superhydrophilic properties of SLActive were due to the interaction of the clean TiO_2 layer with water causing an increase in the surface hydroxy content [23], because the SLActive surface was mainly composed of Ti^{4+} (99.8%). Therefore, it is necessary to compare the hydrophilic properties of plasma oxidation-storage with commercial SLActive in the future.

Studies have shown that, compared with hydrophobic surfaces, the attachment, proliferation, and differentiation of hydrophilic surfaces can be significantly improved in the early stages [27,28]. Therefore, we conclude that the water contact angle, valence state and morphology of the oxidized surface were related to cell responses; that is, a smaller water contact angle leads to better cell adhesion, proliferation, and differentiation. This is consistent with previous research results [13].

In addition, when the isoelectric point (IEP) of a compound is lower than the pH of an aqueous solution, the surface of the compound forms a negative charge due to the dissociation of the surface hydroxyl group (OH) [29]. The IEP values of the TiO_{2-x} surface (about 4–6) [30] have lower pH values than the cell culture medium (about 7) [8]; therefore, oxidation-treated surfaces should be more negatively charged than the untreated SLA surfaces. Alkali treatment also increased surface negative charge. A negatively charged surface facilitates the absorption of Ca^{2+} ions, which in turn attract cell adhesive proteins involved in cell attachment and adhesion [31]. This explains the superior cell adhesion and spreading morphology noted on the surfaces of storage samples. The negative charge of the surface of storage samples should be stronger than that of oxidation samples, resulting in superior cell responses. A similar result showing the positive effects of oxygen plasma immersion ion implantation on the cell responses of titanium materials has previously been reported [8,32].

Significantly higher RTVs and BIC ratios were detected in the Storage group in the second week and fourth week, revealing that the storage implant had faster and better osseointegration at the early healing period compared to the other groups. The RTV indicates the interfacial shear strength between the implant and bone tissue. An increased RTV may lead to an enhancement of superficial bone strength of the bone implant in the storage group, as shown in previous research [33–35]. In addition, the increase in BIC after implantation may be very beneficial for addressing later-stage aseptic loosening of orthopedic and dental prostheses [36,37]. In fact, the active surface, which has increased hydrophilicity and surface free energy, has provided better initial osteoblast cell adhesion onto the implant surface and improved bone-implant integration in the early stages of healing [13–18]. The bone growth results indicate that the combined effects of plasma oxidation and storage in alkali solution can promote the osseointegration of implants and bone, which is vital for primary stability. The results of this study may provide the basis for the treatment and protection of an ideal implant surface.

5. Conclusions

In this study, a highly active TiO_{2-x} gradient interface which has superhydrophilic properties and good biocompatibility was produced by plasma oxidation. However, hydrophilicity and biocompatibility were affected by hydrocarbons in the environment. Therefore, we utilized an alkaline storage method to study the improvement of these characteristics. The surface stored in the alkaline solution retained superhydrophilic and highly active properties and had suitable cell responses. In addition, oxidation and alkali storage treatment resulted in faster and better osseointegration in the early stages of implantation. We conclude that the combination of oxidation and storage methods could improve primary dental implant stability.

Author Contributions: Conceptualization, F.S. and Z.L.; methodology, S.-J.L.; software, F.S.; validation, D.-C.B. and G.-Q.S.; formal analysis, S.-J.L.; investigation, L.W.; resources, Z.L.; data curation, X.-C.L.; writing—original draft preparation, F.S.; writing—review and editing, Z.L.; visualization, S.-J.L.; supervision, Z.L.; project administration, X.-C.L. and C.-S.S. All authors have read and agreed to the published version of the manuscript.

Funding: This research was funded by National Natural Science Foundation of China (No. 51775096); Fundamental Research Funds for the Central Universities, China (No. N2003009); and Chinese Academy of Sciences-WEGO Research Development Plan ([2017]006).

Acknowledgments: The authors would like to thank Bao-hong Zhao research team, Center of Implant Dentistry, School of Stomatology, China Medical University for supporting the experiments.

Conflicts of Interest: The authors declare no conflict of interest.

References

1. Rautray, T.R.; Narayanan, R.; Kim, K.-H. Ion implantation of titanium based biomaterials. *Prog. Mater. Sci.* **2011**, *56*, 1137–1177. [CrossRef]
2. Webster, T.J.T.; Yao, C. Anodization: A Promising Nano Modification Technique of Titanium-Based Implants for Orthopedic Applications. *Surg. Tools Med. Devices* **2016**, *52*, 55–79. [CrossRef]
3. Abdulgani, A.; Muhamad, A.H.; Georges, D.C. Implant Stability: Methods and Recent Advances. *IOSR JDMS* **2017**, *16*, 13–23. [CrossRef]
4. Jeong, S.-J.; Wang, G.; Choi, B.-D.; Hwang, Y.-H.; Kim, B.-H.; Ko, Y.-M.; Jeong, M.-J. Secretory Leukocyte Protease Inhibitor (SLPI) Increases Focal Adhesion in MC3T3 Osteoblast on Titanium Surface. *J. Nanosci. Nanotechnol.* **2015**, *15*, 200–204. [CrossRef]
5. Manara, S.; Paolucci, F.; Palazzo, B.; Marcaccio, M.; Foresti, E.; Tosi, G.; Sabbatini, S.; Sabatino, P.; Altankov, G.; Roveri, N. Electrochemically-assisted deposition of biomimetic hydroxyapatite–collagen coatings on titanium plate. *Inorganica Chim. Acta* **2008**, *361*, 1634–1645. [CrossRef]
6. Jin, G.; Qin, H.; Cao, H.; Qian, S.; Zhao, Y.; Peng, X.; Zhang, X.; Liu, X.; Chu, P.K. Synergistic effects of dual Zn/Ag ion implantation in osteogenic activity and antibacterial ability of titanium. *Biomaterials* **2014**, *35*, 7699–7713. [CrossRef]
7. Mändl, S.; Sader, R.; Thorwarth, G.; Krause, D.; Zeilhofer, H.-F.; Horch, H.; Rauschenbach, B. Biocompatibility of titanium based implants treated with plasma immersion ion implantation. *Nucl. Instrum. Methods Phys. Res. Sect. B Beam Interact. Mater. Atoms* **2003**, *206*, 517–521. [CrossRef]
8. Yang, C.-H.; Li, Y.-C.; Tsai, W.-F.; Ai, C.-F.; Huang, H.-H. Oxygen plasma immersion ion implantation treatment enhances the human bone marrow mesenchymal stem cells responses to titanium surface for dental implant application. *Clin. Oral Implant. Res.* **2013**, *26*, 166–175. [CrossRef]
9. Lin, Z.; Wang, Y.; Wang, D.-N.; Zhao, B.-H.; Li, J.-C. Porous structure preparation and wettability control on titanium implant. *Surf. Coatings Technol.* **2013**, *228*, S131–S136. [CrossRef]
10. Rupp, F.; Scheideler, L.; Olshanska, N.; De Wild, M.; Wieland, M.; Geis-Gerstorfer, J. Enhancing surface free energy and hydrophilicity through chemical modification of microstructured titanium implant surfaces. *J. Biomed. Mater. Res. Part A* **2005**, *76*, 323–334. [CrossRef]
11. Tugulu, S.; Löwe, K.; Scharnweber, D.; Schlottig, F. Preparation of superhydrophilic microrough titanium implant surfaces by alkali treatment. *J. Mater. Sci. Mater. Electron.* **2010**, *21*, 2751–2763. [CrossRef] [PubMed]

12. Jiang, L.; Jin, S.; Geng, S.; Deng, C.; Lin, Z.; Zhao, B. Maintenance and Restoration Effect of the Surface Hydrophilicity of Pure Titanium by Sodium Hydroxide Treatment and its Effect on the Bioactivity of Osteoblasts. *Coatings* **2019**, *9*, 222. [CrossRef]
13. Haibin, L.; Lei, W.; Xueyang, Z.; Mingdeng, R.; Zehong, G.; Lei, Z. Effects of Hydrocarbons Contamination on Initial Responses of Osteoblast-like Cells on Acid-Etched Titanium Surface. *Rare Met. Mater. Eng.* **2013**, *42*, 1558–1562. [CrossRef]
14. Sista, S.; Wen, C.; Hodgson, P.D.; Pande, G. The influence of surface energy of titanium-zirconium alloy on osteoblast cell functions in vitro. *J. Biomed. Mater. Res. Part A* **2011**, *97*, 27–36. [CrossRef] [PubMed]
15. Kopf, B.S.; Ruch, S.; Berner, S.; Spencer, N.D.; Maniura-Weber, K. The role of nanostructures and hydrophilicity in osseointegration: In-vitroprotein-adsorption and blood-interaction studies. *J. Biomed. Mater. Res. Part A* **2015**, *103*, 2661–2672. [CrossRef]
16. Gittens, R.A.; Scheideler, L.; Rupp, F.; Hyzy, S.L.; Geis-Gerstorfer, J.; Schwartz, Z.; Boyan, B.D. A review on the wettability of dental implant surfaces II: Biological and clinical aspects. *Acta Biomater.* **2014**, *10*, 2907–2918. [CrossRef]
17. Preshaw, P. Summary of: Implant surface characteristics and their effect on osseointegration. *Br. Dent. J.* **2015**, *218*, 292–293. [CrossRef]
18. Poon, C.; Hasim, F. Carcinoid tumour metastases to the maxilla. *Int. J. Oral Maxillofac. Surg.* **2007**, *36*, 869–870. [CrossRef]
19. Lang, N.P.; Salvi, G.E.; Huynh-Ba, G.; Ivanovski, S.; Donos, N.; Bosshardt, D. Early osseointegration to hydrophilic and hydrophobic implant surfaces in humans. *Clin. Oral Implant. Res.* **2011**, *22*, 349–356. [CrossRef]
20. Hsu, H.C.; Wu, S.C.; Hsu, S.K. Surface Modification of Commercially Pure Ti Treated with Aqueous NaOH Treatment and Ethyl Alcohol Aging. *J. Med. Biol. Eng.* **2013**, *33*, 331–336. [CrossRef]
21. Lin, Z.; Lee, G.-H.; Liu, C.-M.; Lee, I.-S. Controls in wettability of TiOx films for biomedical applications. *Surf. Coatings Technol.* **2010**, *205*, S391–S397. [CrossRef]
22. Lin, Z.; Li, S.-J.; Sun, F.; Ba, D.-C.; Li, X.-C. Surface characteristics of a dental implant modified by low energy oxygen ion implantation. *Surf. Coatings Technol.* **2019**, *365*, 208–213. [CrossRef]
23. Wall, I.; Donos, N.; Carlqvist, K.; Jones, F.; Brett, P. Modified titanium surfaces promote accelerated osteogenic differentiation of mesenchymal stromal cells in vitro. *Bone* **2009**, *45*, 17–26. [CrossRef] [PubMed]
24. Hotchkiss, K.M.; Ayad, N.B.; Hyzy, S.L.; Boyan, B.; Olivares-Navarrete, R. Dental implant surface chemistry and energy alter macrophage activation in vitro. *Clin. Oral Implant. Res.* **2016**, *28*, 414–423. [CrossRef] [PubMed]
25. Connor, P.A.; Dobson, K.D.; McQuillan, A.J. Infrared Spectroscopy of the TiO_2/Aqueous Solution Interface. *Langmuir* **1999**, *15*, 2402–2408. [CrossRef]
26. Wang, X.; Li, Y.; Liu, X.; Gao, S.; Huang, B.; Dai, Y. Preparation of Ti^{3+} self-doped TiO_2 nanoparticles and their visible light photocatalytic activity. *Chin. J. Catal.* **2015**, *36*, 389–399. [CrossRef]
27. Chou, W.-C.; Wang, R.C.-C.; Huang, C.-L.; Lee, T.-M. The effect of plasma treatment on the osseointegration of rough titanium implant: A histo-morphometric study in rabbits. *J. Dent. Sci.* **2018**, *13*, 267–273. [CrossRef]
28. Raimbault, O.; Benayoun, S.; Anselme, K.; Mauclair, C.; Bourgade, T.; Kietzig, A.-M.; Girard-Lauriault, P.-L.; Valette, S.; Donnet, C. The effects of femtosecond laser-textured Ti-6Al-4V on wettability and cell response. *Mater. Sci. Eng. C* **2016**, *69*, 311–320. [CrossRef]
29. Lu, X.; Wang, Y.; Yang, X.; Zhang, Q.; Zhao, Z.; Weng, L.-T.; Leng, Y. Spectroscopic analysis of titanium surface functional groups under various surface modification and their behaviorsin vitroandin vivo. *J. Biomed. Mater. Res. Part A* **2007**, *84*, 523–534. [CrossRef]
30. Schliephake, H.; Scharnweber, D. Chemical and biological functionalization of titanium for dental implants. *J. Mater. Chem.* **2008**, *18*, 2404. [CrossRef]
31. Bodhak, S.; Bose, S.; Bandyopadhyay, A. Role of surface charge and wettability on early stage mineralization and bone cell–materials interactions of polarized hydroxyapatite. *Acta Biomater.* **2009**, *5*, 2178–2188. [CrossRef] [PubMed]
32. Yang, C.H.; Wang, Y.T.; Tsai, W.F.; Ai, C.F.; Lin, M.C.; Huang, H.H. Effect of oxygen plasma immersion ion implantation treatment on corrosion resistance and cell adhesion of titanium surface. *Clin. Oral Implants Res.* **2011**, *22*, 1426–1432. [CrossRef] [PubMed]

33. Chang, B.; Song, W.; Han, T.; Yan, J.; Li, F.; Zhao, L.; Kou, H.; Zhang, Y. Influence of pore size of porous titanium fabricated by vacuum diffusion bonding of titanium meshes on cell penetration and bone ingrowth. *Acta Biomater.* **2016**, *33*, 311–321. [CrossRef] [PubMed]
34. Zhang, W.; Wang, G.; Liu, Y.; Zhao, X.; Zou, D.; Zhu, C.; Jin, Y.; Huang, Q.; Sun, J.; Liu, X.; et al. The synergistic effect of hierarchical micro/nano-topography and bioactive ions for enhanced osseointegration. *Biomater.* **2013**, *34*, 3184–3195. [CrossRef] [PubMed]
35. Yan, J.; Sun, J.-F.; Chu, P.K.; Han, Y.; Zhang, Y.-M. Bone integration capability of a series of strontium-containing hydroxyapatite coatings formed by micro-arc oxidation. *J. Biomed. Mater. Res. Part A* **2013**, *101*, 2465–2480. [CrossRef]
36. Raphel, J.; Karlsson, J.; Galli, S.; Wennerberg, A.; Lindsay, C.; Haugh, M.G.; Pajarinen, J.; Goodman, S.B.; Jimbo, R.; Andersson, M.; et al. Engineered protein coatings to improve the osseointegration of dental and orthopaedic implants. *Biomaterials* **2016**, *83*, 269–282. [CrossRef]
37. Tejero, R.; Anitua, E.; Orive, G. Toward the biomimetic implant surface: Biopolymers on titanium-based implants for bone regeneration. *Prog. Polym. Sci.* **2014**, *39*, 1406–1447. [CrossRef]